Supplementary Information

Hierarchically Organized Materials with Ordered Mesopores: Adsorption Isotherm and Adsorption-Induced Deformation from Small-Angle Scattering

Lukas Ludescher[a], Roland Morak[a], Stephan Braxmeier[b], Florian Putz[c], Nicola Hüsing[c], Gudrun Reichenauer[b], Oskar Paris[a,*]

[a]*Institute of Physics, Montanuniversität Leoben, Franz-Josef Strasse 18, 8700, Leoben, Austria*
[b]*Bavarian Center for Applied Energy Research, Magdalene-Schoch-Str. 3, 97074 Wuerzburg, Germany*
[c]*Chemistry and Physics of Materials, Paris Lodron University Salzburg, Jakob-Haringer Str. 2a, 5020 Salzburg, Austria*

* Corresponding Author: oskar.paris@unileoben.ac.at

S1. Adsorption isotherms

Nitrogen- and water adsorption isotherms of the hierarchical silica sample are shown in Fig. S1. The modeling of the N_2 isotherms was performed employing the Derjaguin-Broekhoff-deBoer [1,2] model, with the parameters taken from (Ludescher et al. 2019). The micropore filling was described using the Langmuir isotherm [3]. The water isotherm was modeled by making use of the fact that both, N_2 (measured at 77.4 K) and water (measured at 290.15 K) access the same pore volume, thus allowing to estimate the unknown water-silica interaction from the known nitrogen-silica interaction and the given water adsorption isotherm (Ludescher et al. 2019). Notably, the two isotherms differ strongly in the film regime, with the amount adsorbed just before capillary condensation being a factor of two smaller for water as compared to nitrogen. Moreover, in contrast to nitrogen, there seems to be no pronounced

micropore filling at very low pressures. To visualize the difference in the filling characteristics, blue dashed lines in Fig. S1 which denote the specific micropore volume of $0.06\ cm^3(liquid)/g$ (see Table 1 of the main text). For water, the specific volume adsorbed of the micropores is reached at a relative pressure of $p/p_0 \sim 0.15$, while the same volume is filled already at relative pressures $p/p_0 < 0.01\ for\ nitrogen\ adsorption$.

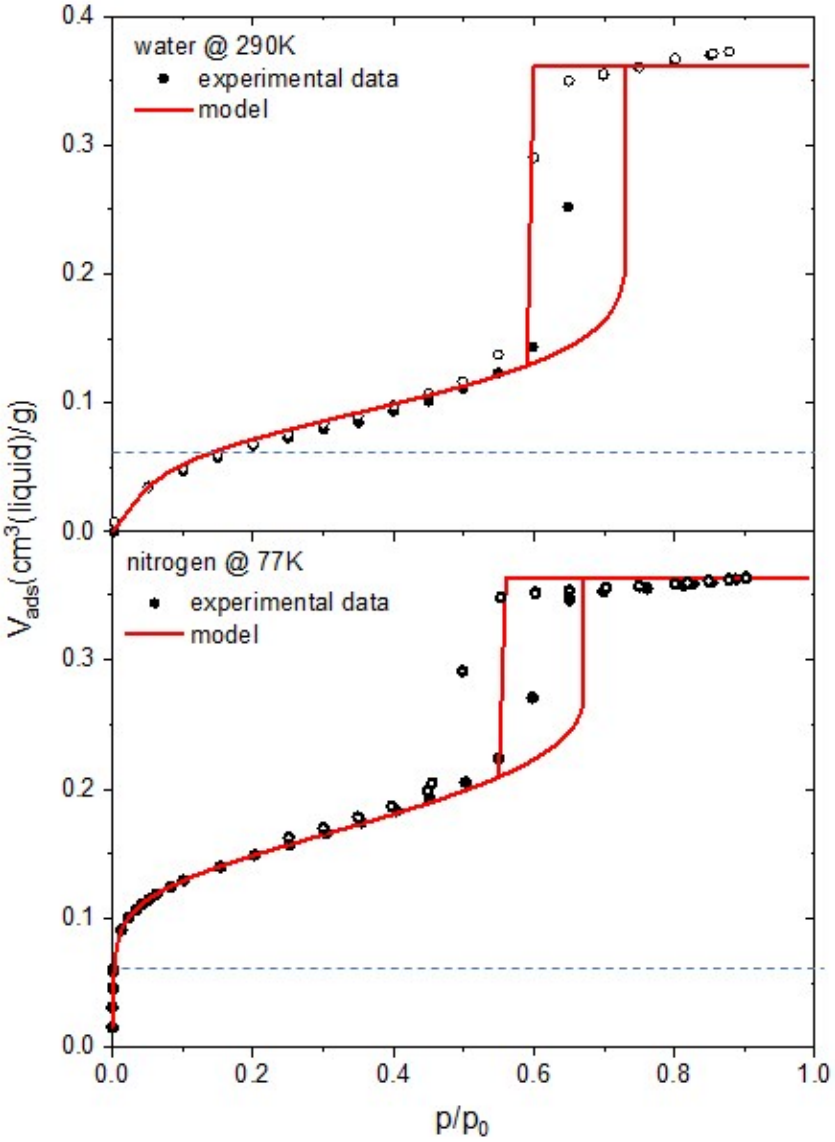

Figure S1: Measured adsorption isotherms of water at 290.15 K (a) and nitrogen at 77.4 K (b) from the hierarchical silica sample calcined at 500°C. Filled symbols denote the adsorption- and open symbols the desorption branches. Modeling of the isotherms using DBdB theory is shown by the solid lines. Blue dashed lines signify the specific micropore volume determined with the t-plot method.

The film thicknesses as a function of relative pressure, used to model the isotherms in Fig. S1 are shown in Fig. S2 for a mesopore radius of 3.3 nm. The film thickness at a given relative pressure is considerably smaller for water as compared to nitrogen, with monolayer coverage being reached only at the relative pressure of $p/p_0 > 0.5$.

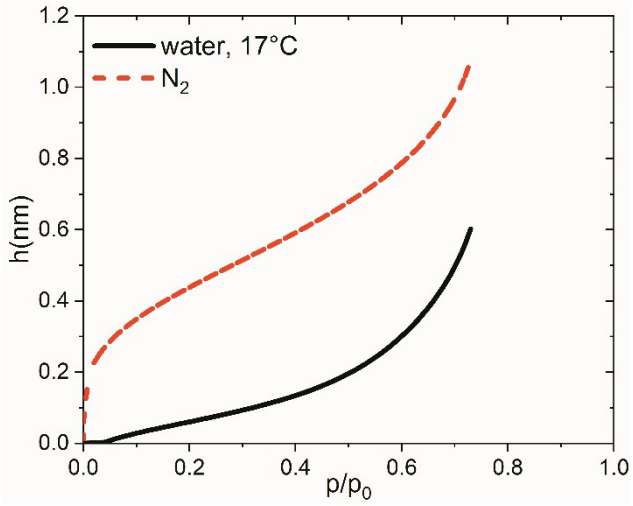

Figure S2: Film thickness of water at 290.15 K (full, black line) and nitrogen at 77.4 K (dashed red line) as a function of relative pressure.

To determine the pore-size distribution (PSD) from the nitrogen adsorption isotherm, the change in the nitrogen specific surface energy was modelled using the Tolman equation, which leads to a so-called 'improved-DBdB' method[4]. This approach allows to determine PSD's with an accuracy similar to NLDFT methods for MCM-41[4]. Using a measured disjoining pressure isotherm[5], a kernel with pore sizes ranging from $r = 1.25\ nm$ to $r = 5\ nm$, with a step-size of $\Delta r = 0.15\ nm$, was calculated and fitted using a constraint on the local curvature of the PSD to obtain a smooth PSD. Prior to fitting, the micropore contribution as a function of relative pressure was calculated by Eq. S1 and subtracted using the appropriate values from Ludescher et al[5]. The PSD resulting from this procedure is shown in Fig. S3a. The mean pore size obtained this way is approximately $2.7\ nm$, with standard deviation of $0.25\ nm$, obtained from the fit with a Gaussian (red line). The mean pore size used in the simulations of the apparent strains was determined from the two-step corona model from SAXS ($3.2\ nm$, see Table 1 in the main text), with the width ($\sigma = 0.3\ nm$) estimated with the procedure described in section S4 below. The mean pore size deduced from SAXS is larger by about 20% as compared to the value from nitrogen adsorption. However, the width of the distributions is very similar for the two different evaluations.

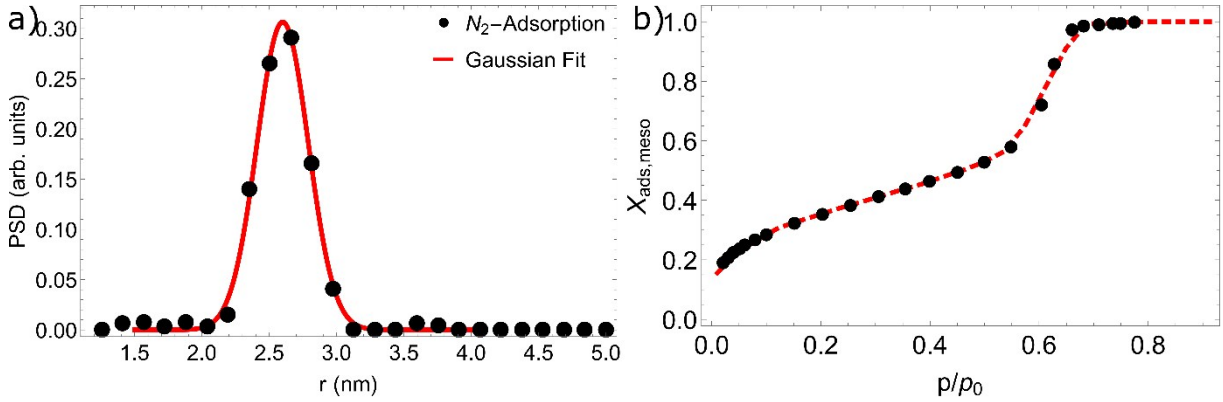

Figure S3: a) Pore size distribution obtained from nitrogen adsorption (symbols) using the iDBdB. The red line is a fit of this PSD with a Gaussian. b) Fit (dashed, red line) of the measured nitrogen adsorption isotherm (symbols) with the iDBdB.

S2. SAXS from micropores

Instead of employing an empirical formfactor function for micropore scattering like in Ref. [6], we describe the micropores by a discrete normal distributed assembly of spherical pores with radius r_μ and standard deviation σ_μ (Eq. 8, main paper). We assume a gradual filling of the micropores with water using the Langmuir isotherm.

$$\gamma_\mu\left(\frac{p}{p_0}\right) = \frac{b\frac{p}{p_0}}{1 + b\frac{p}{p_0}}, \#(S1)$$

Since the interaction parameter b is obtained from the modeling of the adsorption isotherm (Fig. S1) [5], the micropore filling fraction is fully determined (Fig. S4 b) . Because we do not assume any correlation between the micropores, we simply add the scattering intensity from filled and empty micropores according to Eq. 9, main text. The mean size r_μ and size distribution σ_μ of micropores (Table 2, main text) was determined by modeling the scattering pattern of the empty sample using Eq. 6 with the parameters given in Table 1 and Table 2. In Figure S3, the calculated scattering intensity resulting from macro-, meso-, and micropores is shown along with the experimental SAXS pattern at $p/p_0 = 0$. The values obtained for the mean micropore diameter are $2r_\mu = 1.1\ nm$ with variance $\sigma_\mu = 0.28\ nm$. The model fits the experimental SAXS data quite well, except of the peak widths. The reason for this deviation is the limited experimental resolution, which was not taken into account in the model.

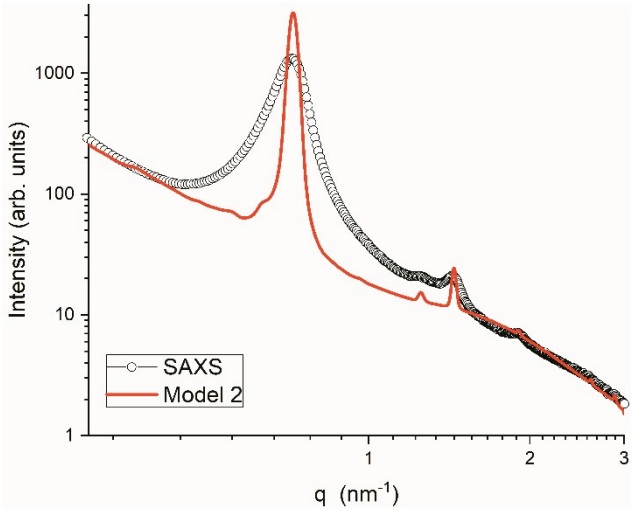

Figure S4: SAXS profile of the empty sample (symbols), together with the modeling of the SAXS curve employing Model 2 (red line).

S3. Derivation of Equation 12 (main manuscript)

To derive Eq. 12 we start from the integrated intensity of a three-phase system [7] for the microporous mesopore wall, which is up to a constant factor related to absolute intensity calibration:

$$\mathcal{I}_{\mu} = \left(\left(\rho_{SiO_2}\right)^2 \phi_{SiO_2}\, \phi_{Void} + \left(\rho_{SiO_2} - \rho_{H_2O}\right)^2 \phi_{SiO_2} \phi_{H_2O} + \left(\rho_{H_2O}\right)^2 \phi_{H_2O}\, \phi_{Void}\right), \#(S2)$$

where the volume fractions ϕ_i and electron densities ρ_i are denoted by their respective subscripts, and

$$\phi_{SiO_2} + \phi_{Void} + \phi_{H_2O} = 1. \#(S3)$$

For the empty micropores $\phi_{Void} = 1 - \phi_{SiO_2}$ ($\phi_{H_2O} = 0$), and for the completely water filled sample $\phi_{H_2O} = 1 - \phi_{SiO_2}$ ($\phi_{Void} = 0$), and with the filling fraction of the pores $x(p/p_0)$ we have

$$\phi_{H_2O}\left(\frac{p}{p_0}\right) = \left(1 - \phi_{SiO_2}\right) x\left(\frac{p}{p_0}\right),$$

$$\phi_{Void}\left(\frac{p}{p_0}\right) = \left(1 - \phi_{SiO_2}\right)\left(1 - x\left(\frac{p}{p_0}\right)\right).$$

Thus Eq. S2 can be written

$$\tilde{I}_{\mu}\left(\frac{p}{p_0}\right) = \rho_{SiO_2}^2 \phi_{SiO_2}\left(1-\phi_{SiO_2}\right)\left(1-x\left(\frac{p}{p_0}\right)\right) + \left(\rho_{SiO_2}-\rho_{H_2O}\right)^2 \phi_{SiO_2}\left(1-\phi_{SiO_2}\right)x\left(\frac{p}{p_0}\right) + \\ + \rho_{H_2O}^2 \phi_{SiO_2}^2 x\left(\frac{p}{p_0}\right)\left(1-x\left(\frac{p}{p_0}\right)\right), \#(S4)$$

which reduces to

$$\tilde{I}_{\mu}(0) = \rho_{SiO_2}^2 \phi_{SiO_2}\left(1-\phi_{SiO_2}\right),$$

and

$$\tilde{I}_{\mu}\left(\frac{p}{p_0}\rightarrow 1\right) = \left(\rho_{SiO_2}-\rho_{H_2O}\right)^2 \phi_{SiO_2}\left(1-\phi_{SiO_2}\right).$$

Because the in-situ SAXS measurements were not scaled to absolute units, we use the ratio of the integrated intensities

$$\frac{\tilde{I}_{\mu}(0)}{\tilde{I}_{\mu}\left(\frac{p}{p_0}\right)} = \frac{\rho_{SiO_2}^2}{\rho_{SiO_2}^2\left(1-x\left(\frac{p}{p_0}\right)\right) + \left(\rho_{SiO_2}-\rho_{H_2O}\right)^2 x\left(\frac{p}{p_0}\right) + \rho_{H_2O}^2 \frac{\phi_{SiO_2}}{1-\phi_{SiO_2}} x\left(\frac{p}{p_0}\right)\left(1-x\left(\frac{p}{p_0}\right)\right)}, \#(S5)$$

which, together with $\phi_{SiO_2} + \phi_{\mu} + \phi_m = 1$ (ϕ_{μ}, ϕ_m being the micro- and mesoporosity, respectively) lead to Eq. 12 in the main text. When applying Eq. 12 to a restricted interval at large q-values, we assume that first the scattering at large q is dominated by micropores, and second that the intensity at a given *q* value is proportional to the integrated intensity. The latter is true, if the micropore filling does not change the shape of the corresponding SAXS profile, but only its pre-factor.

S4. Determining the input parameters for the simulation

Following the procedures outlined in [8,9] the integrated peak intensities of the Bragg reflections from the ordered 2D hexagonal lattice were used to determine the model parameters in Eq. 2, main text. The Bragg peaks were fitted with a Pseudo-Voigt function after transformation

of the measured intensity to a so-called Kratky-representation ($I(q)\ q^2$ is plotted versus q). This representation is advantageous because in it the peak-area is equivalent to the peaks integrated intensity

$$\tilde{I} = 4\pi \int I(q) q^2 dq \#(S6)$$

All fitting procedures were implemented in the method NonlinearModelFit in Mathematica. Here, the squared residual between the input data and a model function is minimized by a simplex method (Nelder-Mead algorithm, achieved by setting *Method → "NMinimize"* in 'NonlinearModelFit). No additional precautions in fitting were needed, as the peak shapes were very well defined by Pseudo-Voigt functions and global minima are automatically sought by "$NMinimize$". For fitting Eq. 2 of the main text, individual weights were assigned to the integrated intensity of each peak. These were defined as the inverse square of the estimated standard deviation of the peaks integrated intensity ($1/\sigma_{hk}^2$, with the standard deviation σ_{hk} determined from the fits of the peak hk). Four Bragg peaks were clearly discernible, namely the (10), (11), (20) and (21) peaks. The inner and outer radii R_1, R_2, as well as the silica fraction of the empty corona $\alpha = \alpha_0$ in Eq. 2 were determined for the empty sample, i.e. for $p/p_0 = 0$ and $\chi = 0$ (Table 1). Then R_1 and R_2 were kept fixed, and $\alpha(p/p_0)$ was determined from the SAXS profiles for relative pressures up to $p/p_0 = 0.65$ (see Fig. S4 a). Above this relative pressure, α was set to the maximum possible value $\alpha_{max} = \alpha_0 + (1 - \alpha_0)\frac{\rho_{H2O}}{\rho_{SiO2}} = 0.755$, i.e., it was assumed that the whole mesopore space within the corona is filled with liquid like water above $p/p_0 = 0.65$. The spontaneous filling of the mesopore space outside the corona was taken into account in the relative pressure interval from the onset of capillary condensation ($p/p_0 = 0.58$) until the complete filling of all mesopores (at $p/p_0 \sim 0.77$) (see Fig. S1). The following expression was used to calculate the form factor

$$F(q) = \left(1 - \Upsilon_m(p/p_0)\right) F_1(q, \alpha, \chi = 0) + \Upsilon_m(p/p_0)\, F_2\left(q, \alpha, \chi = {\rho_{H_2O}}/{\rho_{SiO_2}}\right), \qquad \#(S7)$$

with $\Upsilon_m(p/p_0)$ being the volume fraction of mesopores which have already experienced capillary condensation, and F_1 and F_2 being the form factors according to Eq. 2 below and

above capillary condensation, respectively. The mesopore filling fraction Υ_m obtained from the water adsorption isotherm (Fig. S1) is shown in Fig. S4 b), revealing that capillary condensation extends over a finite pressure range due to a diameter distribution of the mesopores. The mesopore size distribution was estimated in a similar way as described by Müter et al.[10], resulting in a minimum radius of $2\ nm$ at $p/p_0 = 0.58$ and a maximum radius of $3.9\ nm$ at $p/p_0 = 0.77$. Assuming a normal distribution of mesopore radii and interpreting this interval to be of total width $6\sigma_{meso}$, the corresponding width of the mesopore size distribution $\sigma_{meso} = 0.3$ is used as input for the simulation (Table 2, main manuscript). The width estimated using this procedure is in fair agreement with the width estimated from the PSD from nitrogen adsorption, which is $\sigma_{N_2} = 0.25$ (Fig. S3).

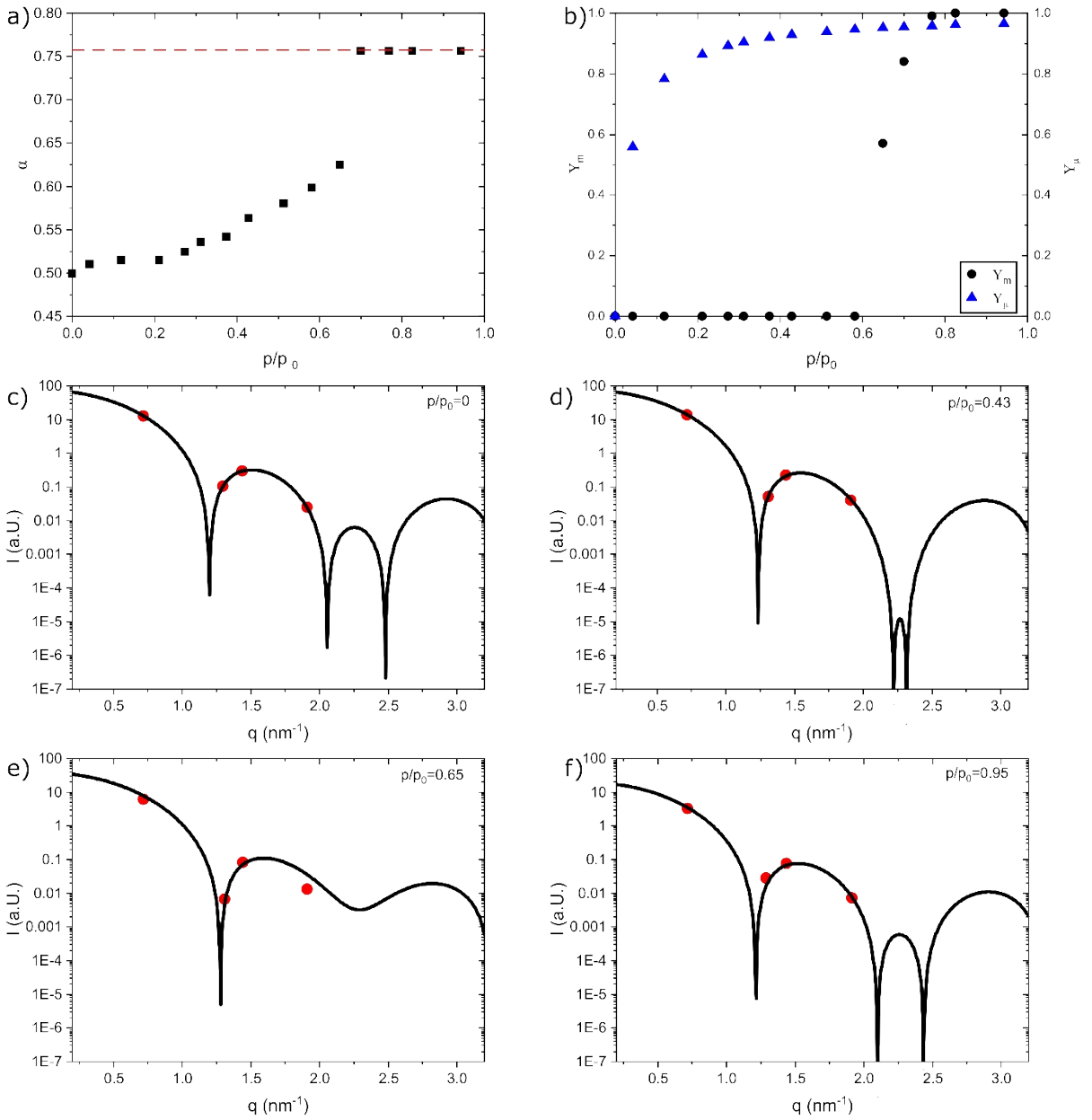

Figure S5: (a): Relative corona density α as function of relative pressure; (b) fraction Υ_m of mesopores in which capillary condensation has occurred (black symbols) and filling fraction of micropores Υ_μ (blue symbols) in. Associated form factor fits (black lines) of integrated peak intensities (red dots) for selected relative pressures are shown in c)-f).

Two different models to determine the electron density distribution inside the mesopres were applied to fit the integrated peak intensities[8]: one where adsorption only occurs in the corona and one where corona filling and an additional liquid film is present. Here we only present the results from the corona model (Fig. S5), as the existence of a liquid film is not needed to satisfactorily fit the integrated intensities of the four discernible peaks. To illustrate the negligible effect of a liquid film, the χ^2- error of both, the 'corona' and the 'corona + film', models are shown for relative pressures below capillary condensation in Figure S6. Throughout all fits the liquid film thickness was at values close to 0 and did not improve, but rather worsen, the fit quality significantly (Fig. S6).

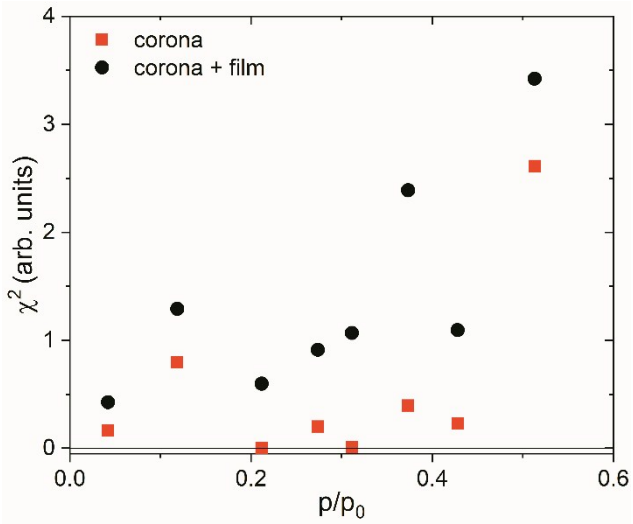

Figure S6: The χ^2- error is shown for two models (pure corona filling as squares, corona filling + liquid film as dots) used to fit the integrated peak intensities of the (10)-, (11)-, (20)- and the (21)-peaks.

S5. Correction for the Porod contribution in the simulations

The form factor for a cylindrical mesopore (Eq. 2) is derived under the assumption that the pore itself is embedded in an infinite silica substrate [8,11]. This means that the strut simulated by employing the Debye-Equation (Eq. 5) is embedded in silica. Because the magnitude of surface scattering from the strut is given by the mean electron density between two separated phases [7], the simulation does not describe the actual surface scattering of a strut surrounded by void space, and needs therefore to be corrected. Since the phase fractions are known for all relative pressures, the Porod-scattering contribution can be analytically calculated [6]:

$$I_{Porod*}(q) = \left(\rho_{SiO_2}\left(\phi_{meso} - \phi_{H_2O}\left(\frac{p}{p_0}\right)\right) + \phi_{H_2O}\left(\frac{p}{p_0}\right)\left(\rho_{SiO_2} - \rho_{H_2O}\right)\right)^2 \frac{A_g}{q^4}, \#(S8)$$

This contribution is subtracted from the mesopore SAXS profiles calculated using the Debye formula (Eq. 5). The correct Porod-scattering calculated using Eq. 7 along with the micropore contribution according to Eq. 8 are then added to the simulated mesopore scattering.

References

1. J. BROEKHOFF, *Journal of Catalysis*, 1967, **9**(1), 8.
2. B. Derjaguin, *Progress in Surface Science*, 1992, **40**(1-4), 46.
3. I. Langmuir, *J. Am. Chem. Soc.*, 1918, **40**(9), 1361.
4. P. Kowalczyk, M. Jaroniec, A.P. Terzyk, K. Kaneko and D.D. Do, *Langmuir*, 2005, **21**(5), 1827.

5. L. Ludescher, R. Morak, C. Balzer, A.M. Waag, S. Braxmeier, F. Putz, S. Busch, G.Y. Gor, A.V. Neimark, N. Huesing, G. Reichenauer and O. Paris, *Langmuir*, 2019, **35**(35), 11590.

6. C.J. Gommes, G. Prieto and P.E. de Jongh, *J. Phys. Chem. C*, 2016, **120**(3), 1488.

7. O. Glatter and O. Kratky, *Small angle x-ray scattering*: *Edited by O. Glatter and O. Kratky,* Academic Press, London, New York, 2nd ed., 1983.

8. G.A. Zickler, S. Jähnert, W. Wagermaier, S.S. Funari, G.H. Findenegg and O. Paris, *Phys. Rev. B*, 2006, **73**(18), 17.

9. M. Impéror-Clerc, P. Davidson and A. Davidson, *J. Am. Chem. Soc.*, 2000, **122**(48), 11925.

10. D. Müter, S. Jähnert, J.W.C. Dunlop, G.H. Findenegg and O. Paris, *J. Phys. Chem. C*, 2009, **113**(34), 15211.

11. M. Impéror-Clerc, *Interface Focus*, 2012, **2**(5), 589.